

Degenerate p orbitals flat band model and realization in two-dimensional materials

Jiang Zeng,¹ Ming Lu,^{2,1} Haiwen Liu,³ Hua Jiang,⁴ and X. C. Xie^{1,2,5}

¹International Center for Quantum Materials, School of Physics, Peking University, Beijing, China

²Beijing Academy of Quantum Information Sciences, Beijing, China

³Center for Advanced Quantum Studies, Department of Physics, Beijing Normal University, Beijing 100875, China

⁴College of Physics, Optoelectronics and Energy, Soochow University, Suzhou 215006, China

⁵CAS Center for Excellence in Topological Quantum Computation, University of Chinese Academy of Sciences, Beijing, China

We propose a flat band model based on degenerate p orbitals at the centers of octahedrons which are closely-packed in a two-dimensional structure. Our theoretical analysis and first-principles calculations show that the proposed flat band can be realized in 1T layered materials of alkali-metal chalcogenides and metal-carbon group compounds. Some of the former are theoretically predicted to be stable as layered materials here (e.g. K_2S), and some of the latter have been experimentally fabricated in previous works (e.g. Gd_2CCl_2). More interestingly, our calculations show that the Gd_2CCl_2 monolayer prefers ferromagnetic order and harbors a spin polarized nearly flat band. Our theoretical model together with the material predictions provide a realistic platform for the realization of flat bands and related exotic quantum phases.

The properties including the electronic bands of a material are codetermined by its structure and the component elements of which the outer-shell electrons usually matter most [1]. In the band theory regime, there are two limiting cases: the massless Dirac fermion in linear dispersion band [2–4] and infinitely heavy fermion in flat band [5, 6]. Both of them harbor unique and fantastic properties. The Dirac fermion has been experimentally realized in a graphene monolayer [3, 4]. For the flat band, the density of states is impressive and effects of interactions are entirely nonperturbative [5–10]. This may offer unique opportunities for the emergence of exotic quantum phases, including ferromagnetism [5–9], high-temperature fractional quantum Hall effect [11–15], Wigner crystallization [16], Bose-Einstein condensation [17], and high-temperature superconductivity [18, 19].

A lot of theoretical models have been proposed to design flat bands [5–9, 11–22]. Some of the most famous models are based on isotropic hopping between orbitals on special lattices [5–9, 20, 21]. For example, two-dimensional (2D) flat bands are theoretically predicted when a decoupled s , p_z , or d_{z^2} orbital is arranged on a kagome lattice, which attracts numerous research interests [5–9]. While seeking for their realization in atomic crystal, it is hard to find a stable material with kagome lattice on which the isotropic orbital is undegenerate and well-isolated from other orbitals [15, 22–24]. Yet to date, definitive experimental demonstrations of electronic flat bands in realistic materials are still lacking. It is still challenging to realize the previous theoretical proposals.

In this Letter, we propose a more realistic flat band model based on the degenerate p orbitals when they site at the centers of octahedrons which are closely-packed to form a 2D structure. Our theoretical analysis and first-principles calculations show that the proposed flat

bands can be realized in 1T layered materials of alkali-metal chalcogenides and metal-carbon group compounds. The calculated flat bands of these materials can be well-described by our theoretical model with physically meaningful parameters. Some of the former materials are theoretically predicted to be stable in layered structure here (e.g. K_2S), while some of the latter have been experimentally fabricated in previous works (e.g. Gd_2CCl_2) [25–27]. More interestingly, our calculations show that the Gd_2CCl_2 monolayer prefers a ferromagnetic order and harbors a spin polarized nearly flat band. Our theoretical model together with the material predictions provide a realistic platform for the realization of flat band and related exotic quantum phases.

We first discuss the tight-binding (TB) model and its

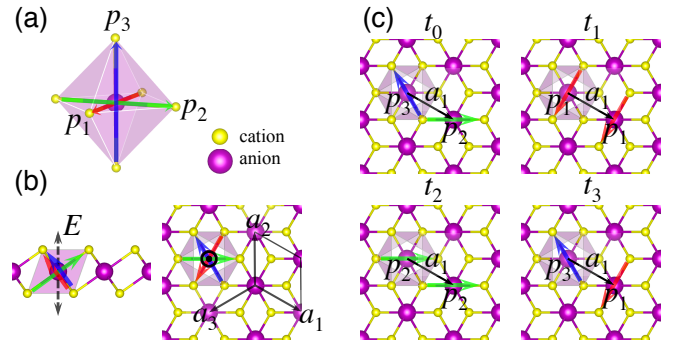


FIG. 1 (color online). The structure and hoppings between p orbitals in a 1T monolayer. (a) An octahedron formed by six cations with an anion at the center. The $p_{1,2,3}$ orbitals on the anion are represented by red, green, and blue arrows, respectively. (b) Schematic diagram of the effective crystal field E . The black rhombus represents one unitcell and black arrows are the lattice vectors $\vec{a}_{1,2,3}$. (c) Schematic diagrams of the hoppings between p orbitals along \vec{a}_1 direction.

single-particle spectrum. In a 1T (tetragonal symmetry, octahedral coordination) layered structure, the octahedrons are closely-packed in 2D planes by sharing edges and corners, as shown in Fig. 1. We define the 2D plane formed by the centers of octahedrons as xy -plane. Three lattice vectors in the xy -plane are defined as $\vec{a}_1 = \frac{\sqrt{3}}{2}a\hat{e}_x - \frac{1}{2}a\hat{e}_y$, $\vec{a}_2 = a\hat{e}_y$, and $\vec{a}_3 = -\vec{a}_2 - \vec{a}_1$, where a is the lattice constant and $\hat{e}_{x,y}$ are the unit vectors of the two orthogonal axes. When an anion locates at the center of an octahedron structure, its three p orbitals are energetically degenerate, as shown in Fig. 1(a). For convenience, we label $p_{x,y,z}$ as $p_{1,2,3}$ and align their polarization direction to the three diagonals of the regular octahedron. Cations locate at the corners of octahedrons to make the system electronically neutral. Here, lattice constant a is also the distance between nearest anions. The TB Hamiltonian $H = H_0 + H'$ reads

$$\begin{aligned}
H_0 &= t_0 \sum_{\vec{r};i;j;k} \{p_{\vec{r},i}^\dagger p_{\vec{r}+\vec{a}_{k,j}} + h.c.\}; \\
H' &= t_1 \sum_{\vec{r};i} \{p_{\vec{r},i}^\dagger p_{\vec{r}+\vec{a}_i} + h.c.\} \\
&+ t_2 \sum_{\vec{r};i;j} \{p_{\vec{r},i}^\dagger p_{\vec{r}+\vec{a}_j,i} (1 - \delta_{i,j}) + h.c.\} \\
&+ t_3 \sum_{\vec{r};i;j} \{(p_{\vec{r},i}^\dagger p_{\vec{r}+\vec{a}_j,j} + p_{\vec{r},i}^\dagger p_{\vec{r}+\vec{a}_i,j}) (1 - \delta_{i,j}) + h.c.\} \\
&+ E \sum_{\vec{r};i;j} p_{\vec{r},i}^\dagger p_{\vec{r},j} (1 - \delta_{i,j}).
\end{aligned} \tag{1}$$

$$\begin{aligned}
&+ t_2 \sum_{\vec{r};i;j} \{p_{\vec{r},i}^\dagger p_{\vec{r}+\vec{a}_j,i} (1 - \delta_{i,j}) + h.c.\} \\
&+ t_3 \sum_{\vec{r};i;j} \{(p_{\vec{r},i}^\dagger p_{\vec{r}+\vec{a}_j,j} + p_{\vec{r},i}^\dagger p_{\vec{r}+\vec{a}_i,j}) (1 - \delta_{i,j}) + h.c.\} \\
&+ E \sum_{\vec{r};i;j} p_{\vec{r},i}^\dagger p_{\vec{r},j} (1 - \delta_{i,j}).
\end{aligned} \tag{2}$$

where $i, j, k = 1 - 3$; \vec{r} runs the locations of all anions in the xy -plane; t_0 describes the hopping between p orbitals on neighboring anions when their polarization directions cross at one corner of the octahedron, namely a cation; t_1 (t_2) describes the neighboring hopping between the same p orbitals when they are (not) perpendicular to the connection direction \vec{a}_i ; t_3 is the hopping between different p orbitals when only one of them is perpendicular to the connection direction \vec{a}_i . E describes the crystal field when the octahedrons are arranged in the 2D plane and the effect of structure adjustment. t_0 is negative due to the odd parity of the p orbitals and atomic potential of cations. The schematic diagrams of the crystal field E and hoppings along \vec{a}_1 direction are shown in Fig. 1(b) and 1(c). The Hermitian conjugate ($h.c.$) describes the hoppings along $-\vec{a}_i$ directions. Due to the existence of cations at the corners of octahedrons, the amplitude of t_0 is usually larger than t_1, t_2, t_3 , and E .

It is of practically guiding significance to consider a limiting case when only t_0 has nonzero value with $t_1 = t_2 = t_3 = E = 0$ and $H = H_0$. In momentum space, we define the three component basis as

$$\psi(\vec{k}) = [p_1(\vec{k}), p_2(\vec{k}), p_3(\vec{k})]^T. \tag{3}$$

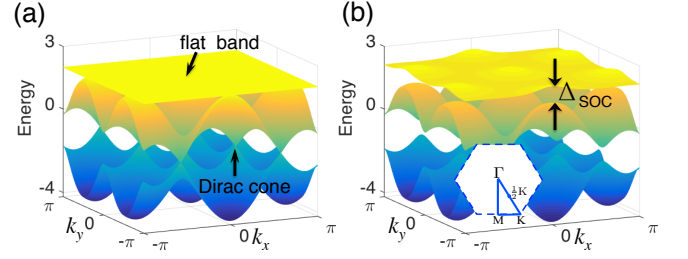


FIG. 2 (color online). Band dispersion of the three degenerate p orbitals with the parameters: (a) $t_0 = -1, t_1 = t_2 = t_3 = E = \lambda = 0$; (b) $t_0 = -1, t_1 = t_2 = t_3 = E = 0, \lambda = 0.2$. In (a), the band E_3 is completely flat, while $E_{1,2}$ exhibit Dirac cones at K points and $\frac{1}{2}$ K points. In (b), the band degeneracy lifts at the high symmetry Γ, M , and K points due to the effects from SOC when $\lambda \neq 0$. Δ_{SOC} in (b) is the direct gap between the nearly flat band E_3 and band E_2 at Γ and M points. The inset in (b) is the Brillouin zone and high-symmetry path.

Then $H(\vec{k})$ takes the matrix form as

$$2t_0 \begin{pmatrix} 0 & \cos(k_3) & \cos(k_2) \\ \cos(k_3) & 0 & \cos(k_1) \\ \cos(k_2) & \cos(k_1) & 0 \end{pmatrix}, \tag{4}$$

where $k_i = \vec{k} \cdot \vec{a}_i$ is defined in the 2D Brillouin zone. The band structure contains three bands $E_{1,2} = t_0 \pm t_0 \sqrt{3 + 2 \sum_i \cos(2k_i)}$ and $E_3 = -2t_0$, as shown in Fig. 2(a). Interestingly, the E_3 band is totally flat over the entire 2D Brillouin zone. On the other hand, the $E_{1,2}$ bands are dispersive exhibiting eight Dirac cones at K and $\frac{1}{2}$ K points in the first Brillouin zone. The bandwidth of $E_{1,2}$ is determined by the amplitude of t_0 . The dispersive band E_2 and flat band E_3 are energetically degenerate at Γ and M points.

With regard to spin-orbit coupling (SOC), we consider the original atomic form: $H_{\text{SOC}} = \lambda \vec{L} \cdot \vec{\sigma}$ [15, 28]. It reads

$$H_{\text{SOC}} = \lambda \begin{pmatrix} -i\sigma_3 & i\sigma_2 \\ i\sigma_3 & 0 & -i\sigma_1 \\ -i\sigma_2 & i\sigma_1 & 0 \end{pmatrix}, \tag{5}$$

where $\sigma_{1,2,3}$ are Pauli matrices [28]. As shown in Fig. 2(b), the band degeneracy lifts at the high symmetry Γ, M , and K points due to the effects from SOC. A global gap occurs, which isolates the flat bands from other bands. The flat band becomes slightly dispersive after taking finite H_{SOC} and H' into consideration.

Based on the above theoretical analysis, a nearly flat band can be realized when H' and H_{SOC} are relatively small or negligible. With the help of first-principles calculations, we predict that two classes of layered materials may harbor nearly flat bands: 1T layered alkali-metal chalcogenides and metal-carbon group compounds. To be specific, we give 1T dipotassium monosulfide

TABLE I. Comparisons of total energies of alkali-metal chalcogenides in different structures. The first row (column) lists the symbol of chalcogens (alkali metals). E_{cubic} , E_{layered} , $E_{1\text{T}}$, and $E_{2\text{H}}$ are calculated total energies per unit cell of the cubic antiferroite, 1T layered bulk, 1T monolayer, and 2H monolayer, respectively. The cubic antiferroite phase is chosen as a reference.

Unit (eV)		O	S	Se	Se
K	$E_{\text{layered}} - E_{\text{cubic}}$	0.58	0.50	0.47	0.43
	$E_{1\text{T}} - E_{\text{layered}}$	0.01	0.18	0.22	0.27
	$E_{2\text{H}} - E_{1\text{T}}$	0.51	0.45	0.42	0.37
Rb	$E_{\text{layered}} - E_{\text{cubic}}$	0.41	0.44	0.40	0.33
	$E_{1\text{T}} - E_{\text{layered}}$	0.09	0.30	0.34	0.42
	$E_{2\text{H}} - E_{1\text{T}}$	0.43	0.39	0.37	0.33

(K₂S) monolayer and digadolinium monocarbide dichloride (Gd₂CCL₂) monolayer as two examples.

Our density functional theory (DFT) calculations are carried out using the Vienna *ab initio* simulation package (VASP) [29], where the projector augmented plane wave (PAW) method [30, 31] is adopted, and the generalized gradient approximation (GGA) in the framework of Perdew-Burke-Ernzerhof (PBE) [32] is chosen for the exchange-correlation interaction. A specific semi-empirical scheme (DFT-D2) [33] is used to treat the van der Waals (vdW) type interaction. Phonon spectrum are obtained using the PHONOPY code [34].

Table I lists the comparisons of total energies of alkali-metal chalcogenides in different structures. The energy difference $E_{\text{layered}} - E_{\text{cubic}}$ describes the relative structural stability of the 1T layered bulk materials to the cubic antiferroite structure. $E_{1\text{T}} - E_{\text{layered}}$ is the exfoliation energy of a 1T monolayer from its layered bulk. The energy difference $E_{2\text{H}} - E_{1\text{T}}$ is the relative structural stability of a 1T monolayer to its 2H (hexagonal symmetry, trigonal prismatic coordination) counterpart. A relatively small and positive value of $E_{\text{layered}} - E_{\text{cubic}}$ means that a layered material may be fabricated experimentally as a metastable phase. A monolayer can be exfoliated from its layered material when the exfoliation energy $E_{1\text{T}} - E_{\text{layered}}$ is small. In Table I, it also shows that all the 1T monolayers are apparently more stable than their 2H counterparts, which benefits the synthesis of high quality 2D samples.

Some of the above 1T monolayered alkali-metal chalcogenides harbor nearly flat bands. As an example, the electronic band structures of the 1T K₂S monolayer are shown in Fig. 3. Our TB model fits well with the DFT calculated band structures with the parameters shown in the caption. Our DFT calculations predict that K₂S can be stabilized in the 1T phase as a monolayered material, which can be confined by the nonnegative phonon spectrum shown in Fig. 3(c). The structure refers to Fig. 1. One S atom sites at the center of an octahe-

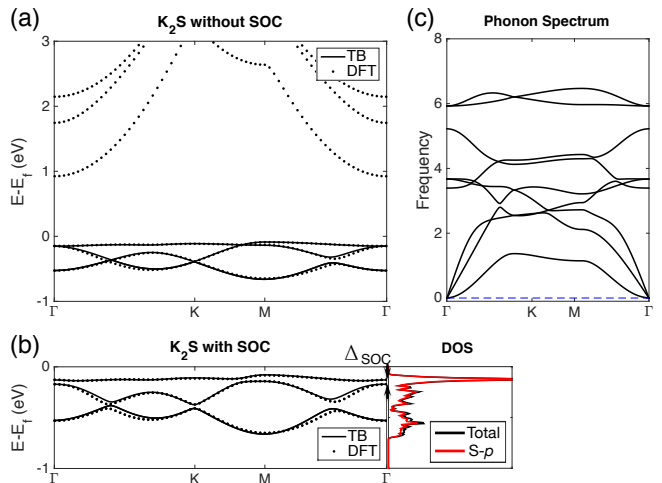


FIG. 3 (color online). Electronic and phonon bands of a 1T K₂S monolayer. Electronic bands (a) without SOC; (b) with SOC. Filled dots and solid curves represent the data from DFT calculations and TB fittings, respectively. The fitting parameters are: $t_0 = -83$, $t_1 = -19$, $t_2 = 0.13$, $t_3 = 5$, $E = 20$ meV. In (b), $\lambda = 20$ meV describes the SOC effect. Fermi level is set to be zero. The highest valence bands are nearly flat with bandwidth of 59 meV in (a) and 55 meV in (b), respectively. $\Delta_{\text{SOC}} = 53$ meV in (b) is the direct gap between the nearly flat band and dispersive band at Γ point. The right panel in (b) is the orbital projected DOS. The black solid curve is the total DOS and the red is contributions from the *p* orbitals of S atoms (S-*p*). (c) Phonon spectrum of a 1T K₂S monolayer.

dron formed by K atoms. Due to the large difference in electronegativity between alkali metals and chalcogens, the 4*s* electron of K atom transfers to 3*p* orbital of S atom. The highest six valence bands with spin degeneracy included are totally contributed from the nearly degenerate 3*p* orbitals of S anion without hybridization with other orbitals, which is important for the validity of our TB model. These bands are primarily contributed from the 3*p* orbitals of S anions, as illuminated in the orbital projected density of states (DOS) in Fig. 3(b). The optimized lattice constant is: $a = 5.01$ Å, and the bond length between nearest K and S atoms is $b = 3.13$ Å. The effective crystal field E is around 20 meV.

Figure 3(a) shows band structures of K₂S without considering SOC effects. The DFT calculated bandwidth of the nearly flat band is 59 meV. As shown in Fig. 3(b), the DOS around the flat band is impressive. The bandwidth can be tuned by adjusting lattice constant. The nearly flat band can be slightly flatter (more dispersive) when increases (decreases) the lattice constant a . The evolution of the band structures can be well-described by our TB model with proper parameters. There is no global band gap between the nearly flat band and the dispersive band. There are degenerate points around the M and Γ points. The degeneracy lifts and a global band

gap opens when the SOC is taken into consideration. A direct band gap Δ_{SOC} at Γ point is about 53 meV, as shown in Fig. 3(c). The SOC also affects the dispersion of the bands. The bandwidth of the nearly flat band slightly decreases from 59 to 55 meV.

As another large family of materials, compounds of metal and carbon group elements can also adopt the 1T layered structure, some of which have been fabricated in experiments [25–27]. It provides more realistic platforms for the study of flat band. A 1T Gd_2CCl_2 monolayer is a typical example. Figure 4(a) shows the structure of a 1T Gd_2CCl_2 monolayer. In the 1T phase, one C atom sites at the inversion symmetry point of an octahedron formed by six Gd atoms, which is a constitutional unit of the 1T layered structure. On each side a 1T structure, there is one layer of Cl anions. The p orbitals of C and Cl anions are full-filled via the electron transfer from Gd atoms, with the C's $2p$ orbitals at the highest valence bands. The $4f$ orbitals of Gd cations are half-filled. Based on our DFT calculations, the half-filled $4f$ orbitals of Gd prefers a ferromagnetic order. The spin polarized band can be described by adding a Zeeman term $H_M = \sigma_3 M$ into the Hamiltonian, where M describes the effective Zeeman field [15].

Figures 4(b) and 4(c) show the spin polarized band structures. The ferromagnetic order of half-filled $4f$ orbitals of Gd cations has effects on the full-filled $2p$ orbitals of C anions making the highest valence bands spin polarized. The effective Zeeman field M is around 40 meV. The fitting parameters are listed in the caption. The highest three valence bands with spin up can be well-fitted by our TB model, as shown in Fig. 4(b). Similar to the case of K_2S , the highest valence band of the spin up electron in Gd_2CCl_2 is very flat with a bandwidth of 197 meV. From the orbital projected DOS, it is clear that the three highest valence bands are mainly contributed from the p orbitals of C anions.

Figure 4(c) shows the band structure of spin down electrons. The trends of the three highest valence bands can be captured by our TB model. For the spin down p orbitals, t_1 and t_2 is comparable to t_0 . All the bands are relatively more dispersive than the spin up case. The highest valence band is partially flat along the path Γ -M. As shown in the orbital projected DOS in Fig. 4(c), the lowest conduction bands mainly contributed from the f electrons of Gd, which is energetically close to the valence bands. The hybridization of C's p orbitals and Gd's f orbitals makes the valence bands slightly deviate from the p orbital based TB model.

Here we emphasize the significance and novelty of our flat band model, its materials realization, and related properties. Unlike the challenging in experimental realization of previous models via designing an isolated isotropic orbital on special lattices (e.g. kagome lattice [8, 15, 23, 24], dice lattice [21], and Lieb lattice [20]), the degenerate p orbitals flat band model predicted here

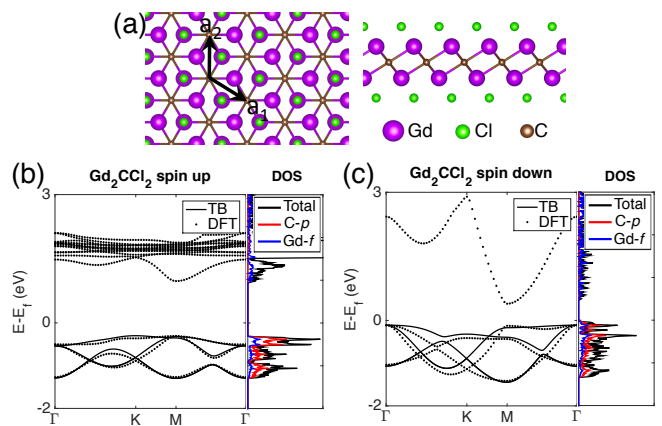


FIG. 4 (color online). The structure and spin-resolved electronic bands of a 1T Gd_2CCl_2 monolayer. (a) The top view and side view of the structure. The electronic bands along high-symmetry paths are shown in (b) for spin up and (c) for spin down, respectively. Filled dots and solid curves represent the data from DFT calculations and TB fittings, respectively. The fitting parameters are: $t_0 = -150$, $t_1 = -40$, $t_2 = -5$, $t_3 = 5$, $E = 30$ meV for spin up; $t_0 = -150$, $t_1 = -100$, $t_2 = 95$, $t_3 = -10$, $E = 20$ meV for spin down; and effective $M = 40$ meV. Fermi level is set to be zero. The right panels in (b) and (c) are the orbital projected DOS. The black, red, and blue curves are the total DOS, contributions from the p orbitals of C atoms (C- p) and f orbitals of Gd atoms (Gd- f), respectively.

can be easily realized. Beyond the two classes of materials predicted above, a lot of 1T layered materials may also have nearly flat band. Compared with the nearly flat band in graphene systems with moiré superlattices [35–37], the DOS around the flat band in the systems predicted here should be much larger making them more intriguing for the study of flat band physics. As the nearly flat band locates at the highest valence band in the K_2S systems, the emergence of magnetic properties can be expected under hole doping. It is worth noting that the Gd_2CCl_2 monolayer intrinsically prefers ferromagnetic order. It may exhibit spin polarized half-metallicity under hole doping [38–40]. The spin polarized flat band may benefit the equal-spin pairing and p -wave superconductivity [41, 42].

In summary, a new TB model with (nearly) flat bands is proposed based on the degenerate p orbitals in 2D materials. Our theoretical analysis and first-principles calculations show that the proposed flat band can be realized in 1T layered materials of alkali-metal chalcogenides and metal-carbon group compounds. The calculated flat bands of these materials can be well-described by our theoretical model with physically meaningful parameters. To be specific, we present 1T K_2S and Gd_2CCl_2 monolayers as two examples. The K_2S monolayer is theoretically predicted to be stable here and the Gd_2CCl_2 layered material has been experimentally fabricated [25]. More

interestingly, our calculations show that the Gd_2CCl_2 monolayer prefers ferromagnetic order and harbors a spin polarized nearly flat band. Our theoretical model together with the material predictions provide a realistic platform for the realization of flat band and related exotic quantum phases.

This work was supported by NBRPC (Grants No. 2015CB921102, No. 2017YFA0303301, and No. 2017YFA0304600) and NSFC (Grants No. 11534001, No. 11504008, No. 11674028, No. 11574245, and No. 11822407).

-
- [1] W. A. Harrison, *Electronic structure and the properties of solids: the physics of the chemical bond* (2012).
- [2] A. C. Neto, F. Guinea, N. M. Peres, K. S. Novoselov, and A. K. Geim, *Reviews of modern physics* **81**, 109 (2009).
- [3] A. K. Geim, *Reviews of Modern Physics* **83**, 851 (2011).
- [4] K. Novoselov, *Reviews of Modern Physics* **83**, 837 (2011).
- [5] A. Mielke, *Journal of Physics A: Mathematical and General* **24**, 3311 (1991).
- [6] H. Tasaki, *Physical review letters* **69**, 1608 (1992).
- [7] A. Mielke, *Journal of Physics A: Mathematical and General* **24**, L73 (1991).
- [8] A. Mielke, *Journal of Physics A: Mathematical and General* **25**, 4335 (1992).
- [9] H. Tasaki, *Progress of Theoretical Physics* **99**, 489 (1998).
- [10] J. D. Bodyfelt, D. Leykam, C. Danieli, X. Yu, and S. Flach, *Physical review letters* **113**, 236403 (2014).
- [11] E. Tang, J.-W. Mei, and X.-G. Wen, *Physical review letters* **106**, 236802 (2011).
- [12] K. Sun, Z. Gu, H. Katsura, and S. D. Sarma, *Physical review letters* **106**, 236803 (2011).
- [13] T. Neupert, L. Santos, C. Chamon, and C. Mudry, *Physical review letters* **106**, 236804 (2011).
- [14] Y.-F. Wang, Z.-C. Gu, C.-D. Gong, and D. Sheng, *Physical review letters* **107**, 146803 (2011).
- [15] Z. Liu, Z.-F. Wang, J.-W. Mei, Y.-S. Wu, and F. Liu, *Physical review letters* **110**, 106804 (2013).
- [16] C. Wu, D. Bergman, L. Balents, and S. D. Sarma, *Physical review letters* **99**, 070401 (2007).
- [17] S. D. Huber and E. Altman, *Physical Review B* **82**, 184502 (2010).
- [18] M. Imada and M. Kohno, *Physical review letters* **84**, 143 (2000).
- [19] S. Peotta and P. Törmä, *Nature communications* **6**, 8944 (2015).
- [20] E. H. Lieb, *Physical review letters* **62**, 1201 (1989).
- [21] F. Wang and Y. Ran, *Physical Review B* **84**, 241103 (2011).
- [22] D. Leykam, A. Andreanov, and S. Flach, *Advances in Physics: X* **3**, 1473052 (2018).
- [23] Z. Lin, J.-H. Choi, Q. Zhang, W. Qin, S. Yi, P. Wang, L. Li, Y. Wang, H. Zhang, Z. Sun, *et al.*, *Physical review letters* **121**, 096401 (2018).
- [24] Z. Li, J. Zhuang, L. Wang, H. Feng, Q. Gao, X. Xu, W. Hao, X. Wang, C. Zhang, K. Wu, *et al.*, *Science advances* **4**, eaau4511 (2018).
- [25] T. Schleid and G. Meyer, *Zeitschrift fur Kristallographie* **209**, 371 (1994).
- [26] M. Ryazanov, A. Simon, and H. Mattausch, *Inorganic chemistry* **45**, 10728 (2006).
- [27] T. Schleid and G. Meyer, *Zeitschrift für anorganische und allgemeine Chemie* **552**, 90 (1987).
- [28] C.-C. Liu, H. Jiang, and Y. Yao, *Physical Review B* **84**, 195430 (2011).
- [29] G. Kresse and J. Furthmüller, *Phys. Rev. B* **54**, 11169 (1996).
- [30] P. E. Blöchl, *Physical review B* **50**, 17953 (1994).
- [31] G. Kresse and D. Joubert, *Physical review b* **59**, 1758 (1999).
- [32] J. P. Perdew, K. Burke, and M. Ernzerhof, *Physical review letters* **77**, 3865 (1996).
- [33] S. Grimme, *Journal of computational chemistry* **27**, 1787 (2006).
- [34] A. Togo and I. Tanaka, *Scr. Mater.* **108**, 1 (2015).
- [35] Y. Cao, V. Fatemi, S. Fang, K. Watanabe, T. Taniguchi, E. Kaxiras, and P. Jarillo-Herrero, *Nature* **556**, 43 (2018).
- [36] Y. Cao, V. Fatemi, A. Demir, S. Fang, S. L. Tomarken, J. Y. Luo, J. D. Sanchez-Yamagishi, K. Watanabe, T. Taniguchi, E. Kaxiras, *et al.*, *Nature* **556**, 80 (2018).
- [37] G. Chen, L. Jiang, S. Wu, B. Lyu, H. Li, B. L. Chittari, K. Watanabe, T. Taniguchi, Z. Shi, J. Jung, *et al.*, *Nature Physics* **15**, 237 (2019).
- [38] T. Cao, Z. Li, and S. G. Louie, *Physical review letters* **114**, 236602 (2015).
- [39] P. Cui, Q. Zhang, H. Zhu, X. Li, W. Wang, Q. Li, C. Zeng, and Z. Zhang, *Physical review letters* **116**, 026802 (2016).
- [40] J. Zeng, W. Chen, P. Cui, D.-B. Zhang, and Z. Zhang, *Physical Review B* **94**, 235425 (2016).
- [41] F. Hardy and A. Huxley, *Physical review letters* **94**, 247006 (2005).
- [42] P. Fulde and R. A. Ferrell, *Physical Review* **135**, A550 (1964).